Struct Multidisc Optim (2015) 51:849–865
DOI 10.1007/s00158-014-1178-8

RESEARCH PAPER

Local continuum shape sensitivity with spatial gradient reconstruction for nonlinear analysis

David M. Cross · Robert A. Canfield

Received: 2 April 2014 / Revised: 21 September 2014 / Accepted: 27 September 2014 / Published online: 7 November 2014

Abstract Gradient-based optimization for large-scale, multidisciplinary design problems requires accurate and efficient sensitivity analysis to compute design derivatives. Presented here is a nonintrusive analytic sensitivity method, that is relatively easy to implement. Furthermore, it can be as accurate as conventional analytic sensitivity methods, which are intrusive and tend to be difficult, if not infeasible, to implement. The nonintrusive local continuum shape sensitivity method with spatial gradient reconstruction (SGR) is formulated for nonlinear systems. This is an extension of the formulation previously published for linear systems. SGR, a numerical technique used to approximate spatial derivatives, can be leveraged to implement the sensitivity method in a nonintrusive manner. The method is used to compute design derivatives for a variety of applications, including nonlinear static beam bending, nonlinear transient gust response of a 2-D beam structure, and nonlinear static bending of rectangular plates. To demonstrate that the method is nonintrusive, all analyses are conducted using black box solvers. One limiting requirement of the method is that it requires the converged Jacobian or tangent stiffness matrix as output from the analysis tool. For each example the design derivatives of the structural displacement response are verified with finite difference calculations.

Keywords Sensitivity analysis · Structural optimization · Fluid-structure interaction · Shape optimization · Aeroelasticity

The views and conclusions contained herein are those of the authors and should not be interpreted as necessarily representing the official policies or endorsements, either expressed or implied, of Air Force Research Laboratory or the U.S. Government.

D. M. Cross (✉) · R. A. Canfield
Aerospace and Ocean Engineering, Virginia Tech, Randolph Hall Room 215 (0203), 460 Old Turner St.,
Blacksburg, VA 24061, USA
e-mail: dmcross@vt.edu

R. A. Canfield
e-mail: bob.canfield@vt.edu

Nomenclature

α_{eff}	Effective angle of attack
$\boldsymbol{A}$	General time-space differential operator
$\boldsymbol{b}$	Design variables
$\boldsymbol{B}$	General boundary operator
C_{L_α}	Lift curve slope
$\boldsymbol{f}$	Body forces)
$\boldsymbol{F}$	Applied load vector
F_f	Quasi-steady lift force
Γ	Spatial boundary
$\boldsymbol{g}$	Applied boundary forces
$[K]$	Stiffness matrix
M	Internal bending moment
N	Internal axial force
Ω	Spatial domain
ψ	Rotational degree of freedom
q_∞	Dynamic pressure
$\boldsymbol{Q}$	Secondary response variables
s	Effective lifting area
t	Time variable
$[T]$	Tangent stiffness matrix
u	x-dispacement
$\boldsymbol{u}$	Primary response variables
U_g	Gust velocity
v	y-displacement
$\boldsymbol{\mathcal{V}}$	Design velocity

V	Internal shear force
w	z-displacement
$\boldsymbol{x}$	Vector of Cartesian coordinates
∇	Gradient operator
$(\cdot)'$	Local design derivative
$\dot{(\cdot)}$	Total design derivative

1 Introduction

In Cross and Canfield (2013) a nonintrusive local continuum shape design sensitivity formulation was presented and implemented for linear transient beam and linear static plate models. The work presented here extends this formulation to nonlinear systems and is implemented for the same models with the inclusion of geometric nonlinearity. This marks the first nonintrusive analytic shape design sensitivity formulation for nonlinear structural problems. By nonintrusive it is meant that the analysis tool can be treated as a black box for which source code is not modified. Successfully implementing gradient-based optimization for large-scale design problems requires an accurate and efficient method for computing design derivatives. The process of calculating design derivatives is commonly referred to as sensitivity analysis, or more specifically as design sensitivity analysis (DSA).

Various methods for conducting DSA may be classified as either numerical or analytical DSA methods. The most common numerical method is the finite difference method. It is very popular because it is nonintrusive, which makes it easy to implement with any analysis tool. However, it is well known that, because this method requires a baseline analysis and an analysis for each perturbed design variable, it is computationally expensive. Furthermore, it can be innaccurate due to roundoff and truncation errors. Therefore, much attention has been given to analytical methods, because they are more efficient and robust than numerical methods, and are often more accurate. However, unlike the finite difference method, analytical methods generally are intrusive.

The intrusive nature of conventional analytic methods stems from the fact that analytic sensitivity equations must be derived by differentiating the governing equations. In addition, the sensitivity equations are specific to approximations made by the analysis tool (e.g. finite element discretization, numerical integration, linearization, etc.). Therefore, analytic methods are typically difficult to implement with general purpose codes, especially for nonlinear analysis, because it requires "intimate knowledge" of how the problem is formulated and solved by the analysis tool (Haftka and Adelman 1989). Oftentimes, this type of information is not provided in the manuals of general purpose analysis tools, making them true black boxes. Furthermore, different models and variable fidelities require separate formulations of the sensitivity equations. The analytical method presented by Cross and Canfield (2013) largely overcomes the disadvantages of conventional analytical methods, because the unique formulation of the local continuum shape sensitivity method is nonintrusive. This work extends that local continuum formulation and fulfills a critical need for a nonintrusive analytic sensitivity method for nonlinear problems. The primary limitation of the nonintrusive method is that it requires access to the Jacobian matrix used by the iterative nonlinear solver. Sometimes the analysis tool may not provide the ability to output the Jacobian matrix. For many CFD codes the Jacobian is never fully assembled or used in any form. Therefore, this method is not immediately applicable to such codes. However, the terms needed to form the tangent stiffness are often computed in many Newton-type solvers. Making use of them nonintrusively, if available, is a topic currently being investigated.

Continuum sensitivity analysis (CSA) is a specific type of analytical sensitivity method. Arora and Haug (1978, 1979), Dems and Mroz (1985), and Dems and Haftka (1989) were among the first to introduce CSA for structural problems. Haug and Arora (1978) were the first to implement CSA for shape design problems. Choi and Kim (2005) extensively documented CSA formulation for structural optimization, and Jameson (1988) pioneered the adjoint formulation of CSA for aerodynamic shape optimzation. Borggaard and Burns (1994, 1997) applied CSA for fluid flow with a direct formulation for aerodynamic design. They followed up this work with other applications of CSA to fluid flow optimization, as did Stanley and Stewart (2002). Turgeon et al. (1999) and Etienne and Pelletier (2005) have applied CSA to numerous fluid-structure interaction (FSI) problems, focusing on sensitivities of fluid flow parameters for nearby problems. Most recently, Wickert, Liu, Canfield, and Cross have employed CSA for shape optimization of nonlinear structures subject to an aeroelastic gust response (Wickert and Canfield 2008; Wickert et al. 2008, 2009; Wickert 2009; Liu and Canfield 2012, 2013a, b; Cross and Canfield 2012a, b).

There are two general classes of CSA, the local continuum method, which poses the sensitivity equations in terms of local design derivatives, and the total continuum method, which poses the sensitivity equations in terms of total design derivatives. The local continuum method is most commonly used by the fluids community, who typically work with Eulerian reference frames. Early on, the structures community largely abandoned the local continuum method, opting for the total continuum method instead. The reason for this was three-fold. First, total design derivatives typically are required for shape design. Second, as discussed by

Liu and Canfield (2013a), the continuity requirements for total derivatives are the same as for the original field variable. Third, the boundary conditions of the local continuum method contain high-order spatial derivatives that can be difficult to accurately recover. However, the total continuum method is intrusive, while the local continuum method provides an opportunity for a nonintrusive formulation. Cross and Canfield (2013) presented a local continuum method that is nonintrusive and eliminates the need to approximate high-order derivatives from primary variable output.

Duvigneau and Pelletier (2006) developed a technique to provide accurate approximations of first- and higher-order spatial derivatives of primary variables, which are used to formulate the boundary conditions of local continuum sensitivity equations (CSEs) for fluid flow applications. Their technique stemmed from work done by Zienkiewicz and Zhu (1992). In this research, as presented by Cross and Canfield (2013), the derivative recovery technique, which is being called spatial gradient reconstruction (SGR), is used to approximate only first-order spatial derivatives, but of both primary and secondary variables. This eliminates the need to recover high-order derivatives of primary variables directly, and enables a nonintrusive local CSA formulation that can be as or more accurate than conventional methods.

The structures community typically opts for total CSA for another reason: the presence of strain discontinuities at structural interfaces causes the local design derivative variables to be discontinuous also. Choi and Kim (2005) and Liu et al. (2010) point out that when using local CSA, special boundary conditions must be enforced at the structural interfaces to account for possible strain discontinuities. This is an inconvenience not inherited by total CSA, but one that must be accepted in order to use the nonintrusive local CSA formulation. An added advantage of local CSA is that the design velocity only needs to be defined on the boundary, and unlike discrete sensitivity analysis, it does not require mesh sensitivities.

The next section extends the local CSA formulation with SGR from Cross and Canfield (2013) to nonlinear analysis. The remaining sections provide several examples where the method is implemented for nonlinear static bending of a 1-D cantilevered beam, nonlinear transient gust analysis of a 2-D beam model, nonlinear static bending of a rectangular plate with out-of-plane loading, and nonlinear static bending of a beam-stiffened rectangular plate with coupled out-of-plane and in-plane loading. All analyses are conducted with black box tools, which demonstrates the nonintrusive nature of the method. The design derivative solutions are compared to finite difference results. Lastly, throughout the paper the advantages as well as the limitations of the method are discussed.

2 Local continuum shape sensitivity formulation

2.1 Governing equations and the material derivative

Figure 1 represents the domain, Ω, in Cartesian space, with essential (geometric) boundary conditions specified on Γ_e, and non-essential (natural) boundary conditions specified on Γ_n of a boudary value problem

$$\boldsymbol{A}(\boldsymbol{u}, t; \boldsymbol{b}) = \boldsymbol{f}(\boldsymbol{x}, t; \boldsymbol{b}) \qquad \text{on} \qquad \Omega \tag{1}$$

$$\boldsymbol{B}(\boldsymbol{u}, t; \boldsymbol{b}) = \boldsymbol{g}(\boldsymbol{x}, t; \boldsymbol{b}) \qquad \text{on} \qquad \Gamma \tag{2}$$

where $\boldsymbol{A}$ and $\boldsymbol{B}$ are the time-space differential operator and the boundary condition operator, respectively. In addition, $\boldsymbol{u} = \boldsymbol{u}(\boldsymbol{x}, t; \boldsymbol{b})$ is a vector of the state or response variables, $\boldsymbol{b}$ is a vector of design variables, $\boldsymbol{x}$ is a vector of spatial coordinates, and t is a temporal variable. The total design derivative of response variables, $\boldsymbol{u}$ with respect to the i-th design parameter, b_i is the material derivative.

$$\frac{D\boldsymbol{u}}{Db_i} = \frac{\partial \boldsymbol{u}}{\partial b_i} + \frac{\partial \boldsymbol{u}}{\partial \boldsymbol{x}} \cdot \frac{\partial \boldsymbol{x}}{\partial b_i} \tag{3}$$

This material derivative consists of the local design derivative, $\frac{\partial \boldsymbol{u}}{\partial \boldsymbol{b}}$, plus a convective term, $\frac{\partial \boldsymbol{u}}{\partial \boldsymbol{x}} \cdot \frac{\partial \boldsymbol{x}}{\partial b_i}$. The convective term captures material movement of the domain, which only occurs when the design variable is a shape parameter. It consists of two parts, spatial derivatives of the response variables and design derivatives of the spatial variables. The latter is often referred to as the design velocity (Arora and Haug 1979; Choi and Kim 2005). Subsequent derivations use the following compact notation of (3) (Wickert and Canfield 2008).

$$\dot{\boldsymbol{u}} = \boldsymbol{u}' + \nabla_{\boldsymbol{x}} \boldsymbol{u} \cdot \boldsymbol{\mathcal{V}} \tag{4}$$

The convective term plays a vital role in local CSA, because it relates the local and total design derivatives to one another. CSA can be conducted using either direct or adjoint

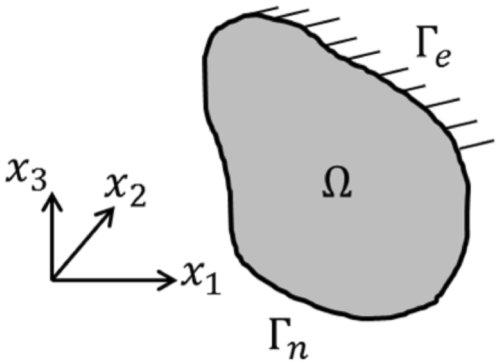

Fig. 1 Domain, Ω, with boundaries Γ_e and Γ_n

formulations. Only the direct method will be discussed here.

2.2 Local continuum shape sensitivity equations

The formulation for linear problems was presented in Cross and Canfield (2013). A convenience of linear problems is that the local CSEs maintain the same left-hand side differential operators as the governing equations. This is not the case for nonlinear problems. By factoring out a $\boldsymbol{u}$ from (1) and (2), the governing equations of the nonlinear boundary value problem can be rewritten as

$$\boldsymbol{A}(\boldsymbol{u}, t; \boldsymbol{b}) = \boldsymbol{A}_{NL}(\boldsymbol{u}, t)\boldsymbol{u} = \boldsymbol{f}(\boldsymbol{x}, t; \boldsymbol{b}) \quad \text{on} \quad \Omega \tag{5}$$

$$\boldsymbol{B}(\boldsymbol{u}, t; \boldsymbol{b}) = \boldsymbol{B}_{NL}(\boldsymbol{u}, t)\boldsymbol{u} = \boldsymbol{g}(\boldsymbol{x}, t; \boldsymbol{b}) \quad \text{on} \quad \Gamma \tag{6}$$

where $\boldsymbol{A}_{NL}$ and $\boldsymbol{B}_{NL}$ are nonlinear differential operators that are functions of $\boldsymbol{u}$. Following the derivation in Cross and Canfield (2013) and being mindful of the chain rule, partial differentiation of (5) yields

$$\left(\boldsymbol{A}_{NL}(\boldsymbol{u}, t)\right)' \boldsymbol{u} + \boldsymbol{A}_{NL}(\boldsymbol{u}, t)\boldsymbol{u}' = \boldsymbol{f}'(\boldsymbol{x}, t; \boldsymbol{b}) \quad \text{on} \quad \Omega \tag{7}$$

where, because $\boldsymbol{A}_{NL}$ has an implicit dependence on $\boldsymbol{b}$ through $\boldsymbol{u}$,

$$\left(\boldsymbol{A}_{NL}(\boldsymbol{u}, t)\right)' = \boldsymbol{A}'_{NL}(\boldsymbol{u}, t) + \frac{\partial \boldsymbol{A}_{NL}}{\partial \boldsymbol{u}}(\boldsymbol{u}, t)\,\boldsymbol{u}' \tag{8}$$

Substitution of this definition and rearrangement yields the local CSE's

$$\left(\boldsymbol{A}_{NL}(\boldsymbol{u}, t) + \frac{\partial \boldsymbol{A}_{NL}}{\partial \boldsymbol{u}}(\boldsymbol{u}, t)\right)\boldsymbol{u}' = \boldsymbol{f}'(\boldsymbol{x}, t; \boldsymbol{b}) - \boldsymbol{A}'_{NL}(\boldsymbol{u}, t)\boldsymbol{u} \quad \text{on} \quad \Omega \tag{9}$$

Total differentiation of (6) yields

$$\left(\dot{\overline{\boldsymbol{B}_{NL}(\boldsymbol{u}, t)}}\right)\boldsymbol{u} + \left(\boldsymbol{B}_{NL}(\boldsymbol{u}, t)\right)\dot{\boldsymbol{u}} = \dot{\boldsymbol{g}}(\boldsymbol{x}, t; \boldsymbol{b}) \quad \text{on} \quad \Gamma \tag{10}$$

where

$$\left(\dot{\overline{\boldsymbol{B}_{NL}(\boldsymbol{u}, t)}}\right) = \boldsymbol{B}'_{NL}(\boldsymbol{u}, t) + \frac{\partial \boldsymbol{B}_{NL}}{\partial \boldsymbol{u}}(\boldsymbol{u}, t)\,\boldsymbol{u}' + \nabla_{\boldsymbol{x}}\left(\boldsymbol{B}_{NL}(\boldsymbol{u}, t)\boldsymbol{u}\right) \cdot \boldsymbol{\mathcal{V}} \tag{11}$$

Equation (10) can be expressed as the local CSE boundary condition by expanding the total design derivatives on the left hand side according to (4) and rearranging terms.

$$\left(\boldsymbol{B}_{NL}(\boldsymbol{u}, t) + \frac{\partial \boldsymbol{B}_{NL}}{\partial \boldsymbol{u}}(\boldsymbol{u}, t)\right)\boldsymbol{u}' = \dot{\boldsymbol{g}}(\boldsymbol{x}, t; \boldsymbol{b}) - \boldsymbol{B}'_{NL}(\boldsymbol{u}, t)\boldsymbol{u} - \nabla_{\boldsymbol{x}}\left(\boldsymbol{B}_{NL}(\boldsymbol{u}, t)\boldsymbol{u}\right) \cdot \boldsymbol{\mathcal{V}} \quad \text{on} \quad \Gamma \tag{12}$$

Equations (9) and (12) are the local CSEs and their sensitivity boundary conditions, respectively. If non-differentiable concentrated loads are present, then they must be defined as domain interfaces with appropriate interface boundary conditions. The governing equations over each domain and all associated boundary conditions can then be differentiated according to (9) and (12).

The static version of the linearized system can be discretized using the Galerkin finite element method to give

$$[K\left(\{u\}^{(r-1)}\right)]\{u\}^{(r)} = \{F\} \tag{13}$$

where u^r denotes the solution at the r-th iteration of the iterative nonlinear solver. Borggaard and Burns (1994), Liu and Canfield (2013c), and Wickert (2009) all showed that, if the same discretization used for the analysis is used to discretize the local CSEs, then the static version of the discretized local CSEs is

$$[T\left(\{u\}\right)]\{u'\} = \{F_{Local}\} \tag{14}$$

where $[T\left(\{u\}\right)]$ is the tangent stiffness matrix of a Newton-Raphson solver and $\{F_{Local}\}$ is the reduced vector of local CSE boundary conditions. The tangent stiffness matrix is defined in relation to the nonlinear stiffness matrix as

$$T_{ij}(u) = K_{ij}(u) + \sum_{m=1}^{n} \frac{\partial K_{im}}{\partial u_j} u_m \tag{15}$$

Notice the similarity between (15) and the left-hand sides of (9) and (12). The only differences between the local CSEs presented in Cross and Canfield (2013) for linear problems and the local CSEs presented here for nonlinear problems are the definitions of the differential operators. The next subsection discusses how this effects the implementation of the local continuum method.

2.3 Implementation and solution of the local continuum sensitivity equations

For linear problems, the analysis tool used to solve the original system can also be used to solve the local CSEs, because the corresponding local CSEs are governed by the same differential operators that appear in the governing equations. After conducting the original analysis, the output can be used to formulate the boundary conditions of the local CSEs. These can then be applied to a second analysis which yields the local design derivative solution. Another option is to solve the local CSEs externally, which requires that the analysis tool provide the system matrices used to solve the original analysis.

It is not as straightforward for nonlinear problems, because the differential operators of the local CSEs are not equivalent to those of the governing equations. Therefore, the primary option is to solve the local CSEs for nonlinear problems externally by having the analysis tool provide the converged tangent matrix, such as the one in (14).

For the essential and non-essential boundary conditions it can be stated that

$$\boldsymbol{B}_{NL}^{(e)}\boldsymbol{u}_{NL} = \boldsymbol{u}_{NL} = \dot{\boldsymbol{g}}_{\Gamma_e}(\boldsymbol{x}, t; \boldsymbol{b}) \quad \text{on} \quad \Gamma_e, \tag{16}$$

and

$$\boldsymbol{B}_{NL}^{(n)}\boldsymbol{u}_{NL} = \boldsymbol{Q}_{NL} = \dot{\boldsymbol{g}}_{\Gamma_n}(\boldsymbol{x}, t; \boldsymbol{b}) \quad \text{on} \quad \Gamma_n \tag{17}$$

where $\boldsymbol{B}_{NL}^{(e)}$ and $\boldsymbol{B}_{NL}^{(n)}$ are the essential and non-essential nonlinear boundary condition operators, respectively, and $\boldsymbol{u}_{NL}$ and $\boldsymbol{Q}_{NL}$ are the primary variable (e.g. displacement) and secondary variable (e.g. element force) responses of the nonlinear analysis, respectively. Assuming that $\boldsymbol{B}'_{NL}$ vanishes from (12) (discussed in Cross and Canfield 2013), it follows that the local CSE boundary conditions for nonlinear problems, can be rewritten as

$$\left(\boldsymbol{B}_{NL}^{(e)}(\boldsymbol{u}_{NL}) + \frac{\partial \boldsymbol{B}_{NL}^{(e)}}{\partial \boldsymbol{u}}(\boldsymbol{u}_{NL})\right)\boldsymbol{u}'_{NL} = \boldsymbol{u}'_{NL} = \dot{\boldsymbol{g}}_{\Gamma_e}(\boldsymbol{x}, t; \boldsymbol{b}) - \nabla_{\boldsymbol{x}}\boldsymbol{u}_{NL} \cdot \boldsymbol{\mathcal{V}} \quad \text{on} \quad \Gamma_e \tag{18}$$

$$\left(\boldsymbol{B}_{NL}^{(n)}(\boldsymbol{u}_{NL}) + \frac{\partial \boldsymbol{B}_{NL}^{(n)}}{\partial \boldsymbol{u}}(\boldsymbol{u}_{NL})\right)\boldsymbol{u}'_{NL} = \boldsymbol{Q}'_{NL} = \dot{\boldsymbol{g}}_{\Gamma_n}(\boldsymbol{x}, t; \boldsymbol{b}) - \nabla_{\boldsymbol{x}}\boldsymbol{Q}_{NL} \cdot \boldsymbol{\mathcal{V}} \quad \text{on} \quad \Gamma_n \tag{19}$$

In order to solve the local CSEs, the system matrix of the original analysis is used as the sensitivity coefficient matrices of the local CSEs. The possibility of saving the decomposed matrix to solve the sensitivity equations for subsequent design variables provides computational efficiency that numerical methods cannot. The $\dot{\boldsymbol{g}}$ terms in boundary conditions (18) and (19) can be formulated directly from the enforced displacements and applied loads. The $\boldsymbol{\mathcal{V}}$ term in boundary conditions (18) and (19) is the design velocity, which can be formulated directly from the geometric parameterization. Lastly, the spatial derivatives that appear in boundary conditions (18) and (19) can be approximated using spatial gradient reconstruction (SGR). The details of implementing SGR, which originated from work previously done by Duvigneau and Pelletier (2006) and Zienkiewicz and Zhu (1992), are provided in Cross and Canfield (2013). In short, Duvigneau and Pelletier (2006) used this approach to recover high-order derivatives of the primary variables, but here, (18) and (19) only require first-order derivatives of both primary and secondary variables. The first-order derivatives of a state or response variable at a particular finite element node are approximated through a least-squares match of the response data and a Taylor series approximation of the response data expanded around the node of interest. The response data that is included in the least-squares match is determined by the definition of a patch. A patch is a local region comprised of nearby finite elements. Qualitatively speaking, the accuracy of SGR is improved by increasing the nodal density of the patches and by increasing the order of the Taylor series expansions. For subsequent examples, illustrations of patches and the corresponding least-squares match are shown.

As discussed in Cross and Canfield (2013) conventional analytic sensitivity methods are intrusive, meaning that formulation of the boundary conditions requires "intimate knowledge" of the source code and numerical formulation (Haftka and Adelman 1989). However, this particular method can be implemented nonintrusively, if the following data can be provided by the analysis tool:

1. linear system matrices and converged tangent system matrices
2. primary variable response data (e.g. displacements)
3. secondary variable response data (e.g. element forces)

If these data can be provided by the analysis tool as output, then the boundary conditions can be formulated nonintrusively. Then, the local CSEs can be solved, and the local design derivative solution can be transformed into a total design derivative solution via (4). A flowchart of the approach is provided below (Cross and Canfield 2013) (Fig. 2).

Conventional implementation of local CSA (Liu and Canfield 2013a) uses only primary variable response data, which results in an intrusive method, because the definition of the boundary condition operator, $\boldsymbol{B}_{NL}$, is required. Furthermore, it results in local CSE boundary conditions that depend on high-order derivatives of the primary variables. Approximation of these high-order derivatives can introduce numerical error into the design derivative solution. As previously mentioned, this is one reason that local CSA has largely been ignored by the structures community. Using the secondary variable response data provides two unique advantages. First, a nonintrusive implementation is achieved, and second, only first-order derivatives need to be approximated. Many analysis tools use techniques to improve the accuracy of the secondary variable response data (MSC Software Corporation 2010), which could result in a more accurate boundary condition formulation.

Furthermore, because conventional methods are intrusive, separate derivations of the local CSEs are required for different models. In contrast, the local CSA with SGR method presented here is nonintrusive and element agnostic. Therefore, if the local CSA with SGR algorithm takes the system matrices, primary variable response data, and secondary variable response data as input, then information redarding the analysis source of the input is not required by the algorithm. For example, the same algorithm can be used for DSA of linear and nonlinear problems; problems that use Euler-Bernoulli or Timoshenko beam theories; or problems solved using different orders of nodal based shape

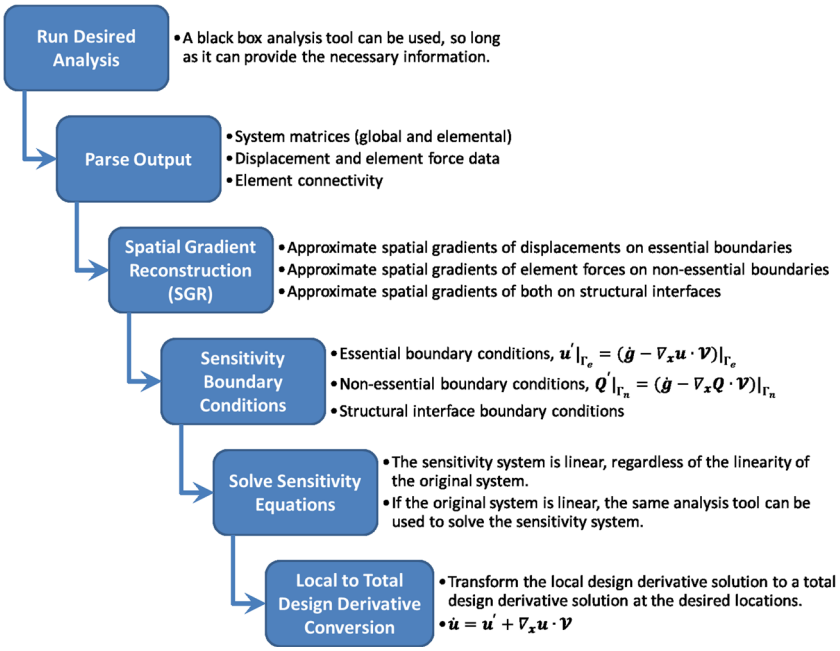

Fig. 2 Detailed flow chart of local continuum shape sensitivity method with spatial gradient reconstruction (Cross and Canfield 2013)

functions. This advantageous characteristic is demonstrated in the remaining sections with several examples.

3 Euler-Bernoulli vs. Timoshenko beam theory

This section presents design derivative results for a short, thick cantilevered beam that is modeled in Nastran (SOL 400) using both Euler-Bernoulli and Timoshenko beam theories (MSC Software Corporation 2010). The beam has Young's modulus, $E = 70GPa$, a shear modulus, $G = 26GPa$, a cross-sectional area, $A = 0.0015m^2$, a area moment of inertia, $I = 4.3\times10^{-5}m^4$, and a shear correction factor, $k_s = 5/6$. The beam, which has a length, $L = 0.5m$, is subjected to an end load, $P = 1MN$. Geometric nonlinearity is included in the analyses. The design derivative of the displacement response is calculated with respect to the length of the beam, L. The design velocity vector, with unit normal coordinate directions $\hat{x}$, $\hat{y}$, and $\hat{z}$, is defined as

$$\boldsymbol{\mathcal{V}} = \frac{x}{L}\hat{x} + 0\hat{y} + 0\hat{z} \tag{20}$$

The sensitivity system is solved in the global reference frame. The global displacement degrees of freedom are $\boldsymbol{u} = \{u, w, \psi\}$, where u is horizontal displacement, w is vertical displacement, and ψ is rotation. The forces are $\boldsymbol{Q} = \{N, V, M\}$, where N is the horizontal force, V is the vertical force, and M is the bending moment. Therefore, the local CSEs simplify to

$$\left(\boldsymbol{A}_{NL}(\boldsymbol{u}) + \frac{\partial \boldsymbol{A}_{NL}}{\partial \boldsymbol{u}}(\boldsymbol{u})\right)\boldsymbol{u}' = 0 \qquad \text{on} \qquad \Omega \tag{21}$$

$$\boldsymbol{u}'(0) = -\nabla_x \boldsymbol{u}(0) \cdot \boldsymbol{\mathcal{V}}(0) = \boldsymbol{0} \tag{22}$$

$$\boldsymbol{Q}'(L) = -\nabla_x \boldsymbol{Q}(L) \cdot \boldsymbol{\mathcal{V}}(L) = -\{N_{,x}(L), V_{,x}(L), M_{,x}(L)\}^T \tag{23}$$

SGR was used to approximate the spatial derivatives that appear in (23) and that appear in the convective term used to transform the local design derivative solution into a total design derivative solution. Five-layer patches and fourth-order Taylor series expansions were used to conduct SGR. Figure 3 illustrates how a five-layer patch and fourth-order Taylor series expansion are used to approximate the first-order spatial derivative of the axial force at the end of the beam.

Both Euler-Bernoulli and Timoshenko beam theory results are shown in Fig. 4, with vertical displacement on

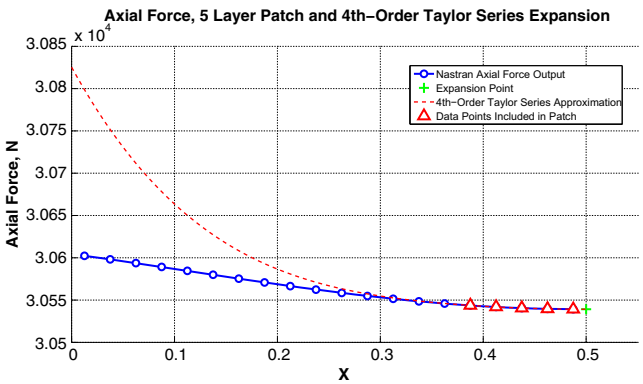

Fig. 3 SGR of axial force employed with a five-layer patch and fourth-order Taylor series expansion

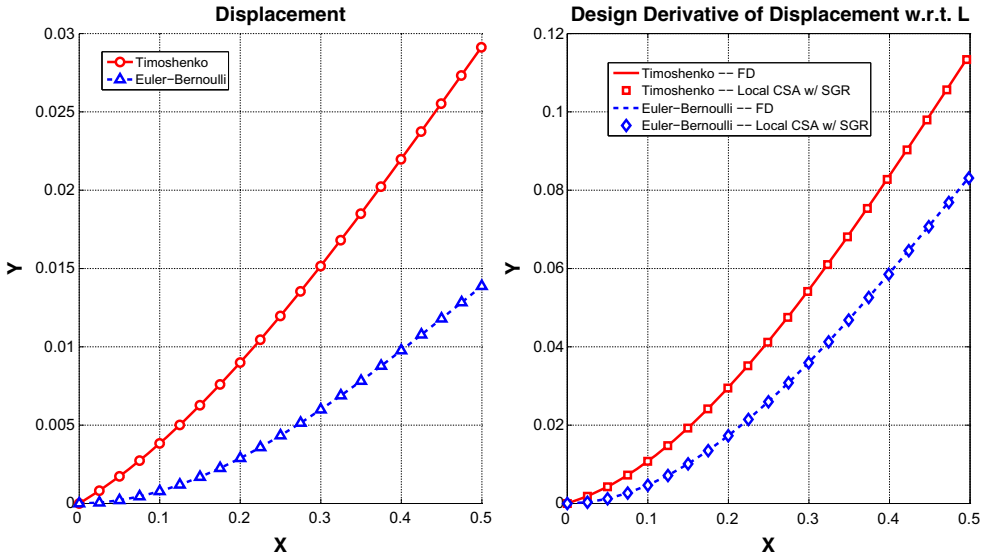

Fig. 4 Vertical displacement (*left*) and design derivative of vertical displacement w.r.t. L (*right*) for a cantilevered beam

the left, and the total design derivative of vertical displacement on the right. Again, the total design derivatives were calculated with respect to the length of the beam, L, and are compared to finite difference results with a relative step size of $10-3$. The displacement results indicate that the Euler-Bernoulli beam behaves more stiffly, because shear effects are neglected. As a result its design derivative solution is less sensitive to the length of the beam. The absolute percent relative difference between the local continuum results and finite difference results were calculated using (24) and are tabulated in Table 1.

$$\epsilon_\phi = \frac{\|\phi_{LC} - \phi_{FD}\|_\infty}{\|\phi_{FD}\|_\infty} \times 100 \tag{24}$$

Here, ϕ is a general design derivative variable, and the subscripts LC and FD indicate coming from the local continuum and finite difference solution, respesctively.

The same algorithm was used for the Euler-Bernoulli and Timoshenko design derivative calculations. Although, different nonlinear operators are used for the analyses, the same type of data feeds into the local CSA with SGR algorithm. Conventional analytic sensitivity methods would require different calculations, based on the specific definitions of the nonlinear operators. For this reason, the nonintrusive nature of this method is advantageous. Furthermore, so long as accurate derivative approximations can be made using SGR, then one can expect similarly accurate design derivative solutions (Cross and Canfield 2013).

Table 1 Absolute percent relative difference of design derivative results

ϵ	$\dot{u}$	$\dot{w}$	$\dot{\psi}$
Timoshenko	0.142	0.081	0.030
Euler-Bernoulli	0.234	0.109	0.029

4 Nonlinear transient gust response of 2-D beam model

4.1 Model information

The joined-beam model presented in Cross and Canfield (2013) is again presented here, but is now modeled using a nonlinear transient gust analysis. Liu et al. (2010) introduced the aeroelastic model shown in Fig. 5 in the context of CSA. The model consists of a long and slender cantilevered beam with a typical section airfoil mounted at the free end. An angled bracing member supports the cantilevered beam. The aeroelastic structure is submerged in a free stream flow and during a specified period of time encounters a one-minus-cosine vertical gust load. The system is aeroelastic because the beam deformation and the aerodynamic load are coupled. The objective is to compute the design derivatives of the transient gust response with respect to the length of the cantilevered beam, L. The geometry is parameterized such that the angle, β, remains constant for a perturbation in

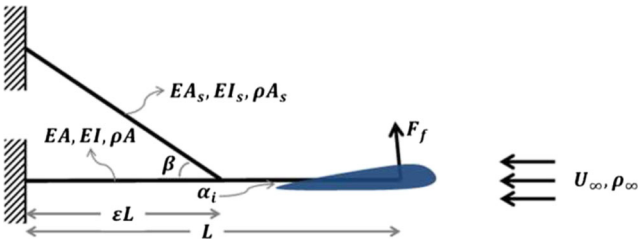

Fig. 5 Typical section airfoil mounted on the free end of a braced cantilever beam

L. The angle, β has been treated as a shape variable by Liu and Canfield (2013a).

In Cross and Canfield (2013) the linear aeroelastic gust response was calculated using Nastran's OpenFSI interface. This allows Nastran's SOL 400 transient solver to communicate with an externally defined C++ code, where the quasi-steady aerodynamics load is defined (MSC Software Corporation 2010). The local CSEs were then solved outside of Nastran using a linear transient solver. This required Nastran to provide the mass matrix, the converged tangent stiffness matrices (global and elemental) at each time step, and the time histories of displacements and element forces. Unfortunately, for the nonlinear transient gust problem, Nastran does not provide element forces as output. Therefore, Nastran does not meet the previously defined requirements for the nonlinear transient problem. A nonlinear transient aeroelastic analysis tool, provided by Liu and Canfield (2013a), was used to compute the nonlinear gust response and design derivative results shown here. This tool was treated entirely as a black box, but was chosen because it could provide the necessary output data required to perform local CSA with SGR.

4.1.1 The structural parameters

The cantilevered beam has the following properties: the length of the beam, $L = 6m$, the axial stiffness, $EA = 1.0556 \times 10^8 N$, the bending stiffness, $EI = 3.0023 \times 10^6 Nm^2$, the shear stiffness, $GA = 3.9208 \times 10^7 N$, the shear correction factor, $k = 5/6$, the mass per unit length, $\rho A = 307 kg/m$, and the mass moment of inertia, $I_m = 52.4\ kg\ m^2$. The properties of the bracing member (strut) are: the strut angle, $\beta = 45^o$, the strut location, $\epsilon = 1/2$, the axial stiffness, $EA_s = 7 \times 10^6 N$, the bending stiffness, $EI_s = 6.5023 \times 10^4 Nm^2$, the mass per unit length, $\rho A_s = 34 N/m$, and the mass moment of inertia, $I_{m_s} = 1.3\ kg\ m^2$.

4.1.2 The typical section aerodynamics

The lift force, $F_f(t)$, is modeled using typical section, quasi-steady aerodynamics.

$$F_f(t) = q_\infty s C_{l_\alpha} \alpha_{eff}(t) \tag{25}$$

In (25), q_∞ is the dynamic pressure, $s = 6m^2$ is the effective lifting area (the chord multiplied by the span of the airfoil section), C_{l_α} is the lift curve slope, and α_{eff} is the effective angle of attack. The dynamic pressure is defined as

$$q_\infty = \frac{1}{2}\rho_\infty U_\infty^2 \tag{26}$$

where, ρ_∞ is the air density and U_∞ is the free stream velocity. The effective angle of attack is defined as

$$\alpha_{eff} = \alpha_i + \theta_{tip} + \frac{U_g}{U_\infty} + \frac{h_{,t}}{U_\infty} \tag{27}$$

In (27), α_i is the incidence angle of attack (orientation of the airfoil relative to the beam frame), θ_{tip} is the rotation of the beam at the free end, U_g is the gust velocity, and $h_{,t}$ is the plunge velocity at the free end of the beam. The plunge velocity has a damping effect, which causes the gust response to dissipate, returning the system to the steady state solution. The gust velocity is defined as

$$U_g(t) = \begin{cases} \frac{1}{2} U_{g,max} \left(1 - \cos\left(\frac{2\pi(t-\tau_i)}{\tau_f}\right)\right) & \tau_i \le t \le \tau_f \\ 0 & \text{otherwise} \end{cases} \tag{28}$$

The aerodynamic parameters are the air density, $\rho_\infty = 1.2 kg/m^3$, the free stream velocity, $U_\infty = 70 m/s$, the effective lifting area, $s = 6m$, the lift curve slope, $C_{l_\alpha} = 2\pi$, the incidence angle of attack, $\alpha_i = 3^o$, the peak gust velocity, $U_{g,max} = 20 m/s$, and the gust period, $\tau_i = 3s$ and $\tau_f = 4s$.

4.2 Design derivative results

The design velocity takes the same definition as the previous example, (20), and the system has the same degrees of freedom, $\boldsymbol{u} = \{u, w, \psi\}$ and $\boldsymbol{Q} = \{N, V, M\}$. The local CSEs also take a similar form, only now they are dynamic equations.

$$\left(\boldsymbol{A}_{NL}(\boldsymbol{u}, t) + \frac{\partial \boldsymbol{A}_{NL}}{\partial \boldsymbol{u}}(\boldsymbol{u}, t)\right)\boldsymbol{u}' = 0 \qquad \text{on} \qquad \Omega \tag{29}$$

$$\boldsymbol{u}'(0, t) = -\nabla_{\boldsymbol{x}} \boldsymbol{u}(0, t) \cdot \boldsymbol{\mathcal{V}}(0) = \boldsymbol{0} \tag{30}$$

$$\begin{aligned} \boldsymbol{Q}'(L, t) &= \dot{\boldsymbol{g}}(L, t) - \nabla_x \boldsymbol{Q}(L, t) \cdot \boldsymbol{\mathcal{V}}(L) \\ &= \{-N_{,x}(L, t), \dot{F}_f(t) - V_{,x}(L, t), -M_{,x}(L, t)\}^T \end{aligned} \tag{31}$$

where the total design derivative of the aeroelastic load, $\dot{F}_f$ is defined as

$$\begin{aligned} \dot{F}_f(t) &= q_\infty s C_{l_\alpha} \left(\dot{\theta}_{tip} + \tfrac{1}{U_\infty}\dot{h}_{,t}\right) \\ &= q_\infty s C_{l_\alpha} \left(\psi' + \psi_{,x} + \tfrac{1}{U_\infty}\left(-w_{,t}' - w_{,tx}\right)\right)\Big|_{x=L} \end{aligned} \tag{32}$$

Furthermore, strain discontinuities at the joint of the main beam and the strut require the following boundary conditions to be enforced. Details concerning these boundary conditions can be found in Liu and Canfield (2013a).

$$\boldsymbol{u}'(x_j^+) = \boldsymbol{u}'(x_j^-) - \left(\boldsymbol{u}_{,x}(x_j^+) - \boldsymbol{u}_{,x}(x_j^-)\right)\boldsymbol{\mathcal{V}}(x_j) \tag{33}$$

$$\boldsymbol{Q}'(x_j) = -\sum \boldsymbol{Q}_{,x}(x_j)\boldsymbol{\mathcal{V}}(x_j) \tag{34}$$

where x_j is the joint location and is equal to ϵL and $\epsilon = 1/2$. A $()^+$ indicates the evaluation is from the right, and a $()^-$ indicates the evaluation is from the left. These boundary conditions require that SGR be used to reconstruct spatial derivatives of $\boldsymbol{u}$ from both the left and right sides of the joint and $\boldsymbol{Q}$ from each of the three structural elements adjacent to the joint. When conducting SGR to approximate these terms, it is essential that the patches are adjacent to the joint, but do not cross over it. This is necessary to capture any discontinuities that may be present.

A more detailed derivation of the local CSEs is included in Cross and Canfield (2013). The results are shown in Fig. 6 with vertical displacement on the left and the design derivative of vertical displacement on the right. Again, design derivatives were calculated with respect to the length of the beam, L, and are validated by comparison to finite difference results (10^{-3} was the converged step size). In addition to the results for the nonlinear gust response, the results for the linear gust response presented in Cross and Canfield (2013) are also shown. Four-layer patches and third-order Taylor series expansions were used to conduct SGR. Furthermore, the same linear transient solver was used to solve the local CSEs for both the linear and nonlinear gust problems.

The relative difference between the local CSA and finite difference solutions is calculated for the time integrated design derivative of nonlinear displacement at both the end of the beam

$$\frac{\int_0^t \dot{w}_{LC}(L,t)dt - \int_0^t \dot{w}_{FD}(L,t)dt}{\int_0^t \dot{w}_{FD}(L,t)dt} = 0.0198 \tag{35}$$

and the joint location.

$$\frac{\int_0^t \dot{w}_{LC}(x_J,t)dt - \int_0^t \dot{w}_{FD}(x_J,t)dt}{\int_0^t \dot{w}_{FD}(x_J,t)dt} = 0.0578 \tag{36}$$

The finite element model consisted of 40 beam elements, and the time integration consisted of 1500 time steps. When investigated this 40 element mesh under static loading for linear analysis, it was determined that four-layer patches and third-order Taylor series produced the most accurate results. Any more layers pollute the SGR calculations with truncation error, becuase the data points are relatively far from the expansion point. Therefore, four-layer patches and third-order Taylor series were assumed to be the best SGR parameters for local CSA of the linear and nonlinear transient gust responses. A finite element mesh with more degrees of freedom would certainly improve the accuracy but at an additional cost. Furthermore, the linear and nonlinear analyses are sufficiently converged using 1500 time

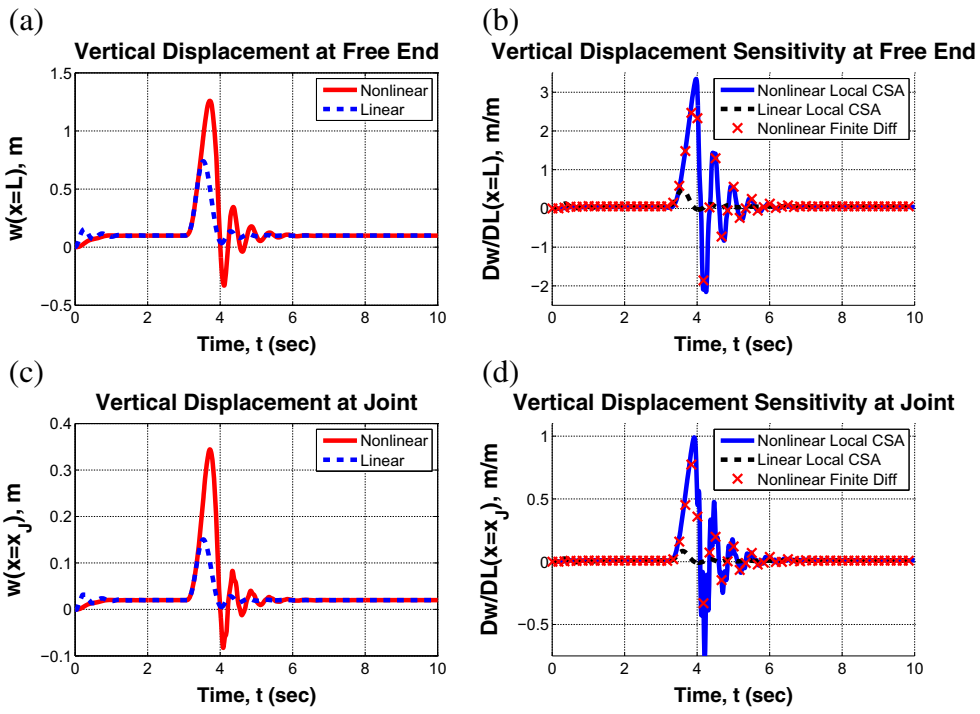

Fig. 6 Joined-beam aeroelastic gust response. **a** Vertical displacement at free end **b** Sensitivity of vertical displacement at free end w.r.t. length, L **c** Vertical displacement at joint **d** Sensitivity of vertical displacement at joint w.r.t. length, L

steps. However, a finer temporal mesh of 2000 time steps reduced the relative differences reported in (35) and (36) to 0.0132 and 0.036 respectively.

The linear and nonlinear responses are critically different. During the gust response, the bracing member (strut) exhibits dramatic geometric nonlinearity, which minimizes its load carrying capability. This softening effect results in very large displacements and rotations, which are illustrated in Fig. 7. The maximum vertical displacement that occurs during the nonlinear response is approximately 70 percent larger than that of the linear response. This is the same type of behavior that was determined to be a critical design condition for HALE aircraft such as Helios (NASA 2004) and Sensorcraft (Johnson 2001). Furthermore, the design derivative results indicate that the nonlinear repsonse is significantly more sensitive to the geometry of the joined beam configuration than the linear response. The maximum total design derivative of vertical displacement that occurs during the nonlinear response is approximately 560 percent larger than that of the linear response. This is further evidence that an accurate and efficient design derivative capability is necessary for such nonlinear models.

5 Nonlinear static plate bending

5.1 Rectangular plate with mixed boundary conditions

The plate model from Section 5.2 of Cross and Canfield (2013), which has two clamped edges and two simply-supported edges, is modeled in Nastran with geometric nonlinearity included. The in-plane degrees of freedom are coupled with the out-of-plane degrees of freedom for the nonlinear problem. The plate lies in the x-y plane with x-dimension, $a = 1m$ and y-dimension, $b = 1.5m$. The magnitude of the uniformly distributed out-of-plane load is $q_0 = 100000N/m^2$, and the plate has Young's modulus, $E = 7e10N/m^2$; thickness, $t = 0.01m$; and Poisson's ratio, $\nu = 0.25$. The edges along $x = 0$ and $x = a$ are simply-supported, while the edges along $y = 0$ and $y = b$ are clamped. Design derivatives of the displacement response are calculated with respect to the plate dimension a. Therefore, the design velocity takes the form

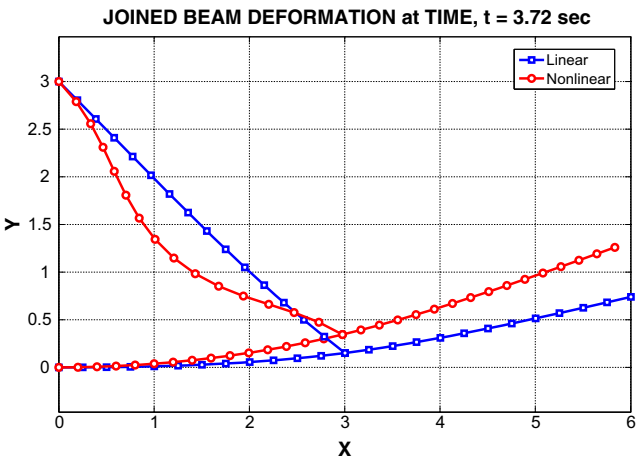

Fig. 7 Joined-beam deflection during the gust response at t = 3.72 seconds (*blue*: linear response, *red*: nonlinear response)

$$\boldsymbol{\mathcal{V}}(x, y; a) = \boldsymbol{\mathcal{V}}_x \hat{x} + \boldsymbol{\mathcal{V}}_y \hat{y} = \frac{x}{a}\hat{x} \tag{37}$$

The displacement degrees of freedom are $\boldsymbol{u}(x, y) = \{u, v, w, \psi_x, \psi_y\}^T$, where u and v are in-plane displacements, w is the out-of-plane displacement, and ψ_i is the rotation about the i-th axis. For this example the rotation about the z-axis (drilling degree of freedom) is held fixed. The forces are $\boldsymbol{Q}(x, y) = \{N_x, N_y, V, M_x, M_y\}^T$, where N_i is axial force in the i-th direction, V is through-thickness shear force, and M_i is the bending moment acting on a face whose outward normal is in the i-th direction. The uniformly distributed transverse load is not dependent on the shape change, thus $f' = 0$, and the local CSEs are

$$\left(\boldsymbol{A}_{NL}(\boldsymbol{u}) + \frac{\partial \boldsymbol{A}_{NL}}{\partial \boldsymbol{u}}(\boldsymbol{u})\right)\boldsymbol{u}' = 0 \qquad \text{on} \qquad \Omega \tag{38}$$

Cross and Canfield (2013) derive the local CSEs for a linear static plate problem where the load is shape dependent. The local CSE boundary conditions along $x = 0$ are

$$u'(0, y) = \dot{u}(0, y) - u_{,x}(0, y)\mathcal{V}_x(0, y) = 0 \tag{39}$$

$$v'(0, y) = \dot{v}(0, y) - v_{,x}(0, y)\mathcal{V}_x(0, y) = 0 \tag{40}$$

$$w'(0, y) = \dot{w}(0, y) - w_{,x}(0, y)\mathcal{V}_x(0, y) = 0 \tag{41}$$

$$\psi_x'(0, y) = \dot{\psi}_x(0, y) - \psi_{x,x}(0, y)\mathcal{V}_x(0, y) = 0 \tag{42}$$

$$M_x'(0, y) = \dot{M}_x(0, y) - M_{x,x}(0, y)\mathcal{V}_x(0, y) = 0 \tag{43}$$

The local CSE boundary conditions along $x = a$ are

$$u'(a, y) = \dot{u}(a, y) - u_{,x}(a, y)\mathcal{V}_x(a, y) = -u_{,x}(a, y) \tag{44}$$

$$v'(a, y) = \dot{v}(a, y) - v_{,x}(a, y)\mathcal{V}_x(a, y) = -v_{,x}(a, y) \tag{45}$$

$$w'(a, y) = \dot{w}(a, y) - w_{,x}(a, y)\mathcal{V}_x(a, y) = -w_{,x}(a, y) \tag{46}$$

$$\psi_x'(a, y) = \dot{\psi}_x(a, y) - \psi_{x,x}(a, y)\mathcal{V}_x(a, y) = -\psi_{x,x}(a, y) \tag{47}$$

$$M'_x(a,y) = \dot{M}_x(a,y) - M_{x,x}(a,y)\mathcal{V}_x(a,y) = -M_{x,x}(a,y) \tag{48}$$

The local CSE boundary conditions along $y = 0$ are

$$u'(x,0) = \dot{u}(x,0) - u_{,x}(x,0)\mathcal{V}_x(x,0) = -u_{,x}(x,0)\frac{x}{a} \tag{49}$$

$$v'(x,0) = \dot{v}(x,0) - v_{,x}(x,0)\mathcal{V}_x(x,0) = -v_{,x}(x,0)\frac{x}{a} \tag{50}$$

$$w'(x,0) = \dot{w}(x,0) - w_{,x}(x,0)\mathcal{V}_x(x,0) = -w_{,x}(x,0)\frac{x}{a} \tag{51}$$

$$M'_y(x,0) = \dot{M}_y(x,0) - M_{y,x}(x,0)\mathcal{V}_x(x,0) = -M_{y,x}(x,0)\frac{x}{a} \tag{52}$$

$$\psi'_y(x,0) = \dot{\psi}_y(x,0) - \psi_{y,x}(x,0)\mathcal{V}_x(x,0) = -\psi_{y,x}(x,0)\frac{x}{a} \tag{53}$$

Lastly, The local CSE boundary conditions along $y = b$ are

$$u'(x,b) = \dot{u}(x,b) - u_{,x}(x,b)\mathcal{V}_x(x,b) = -u_{,x}(x,b)\frac{x}{a} \tag{54}$$

$$v'(x,b) = \dot{v}(x,b) - v_{,x}(x,b)\mathcal{V}_x(x,b) = -v_{,x}(x,b)\frac{x}{a} \tag{55}$$

$$w'(x,b) = \dot{w}(x,b) - w_{,x}(x,b)\mathcal{V}_x(x,b) = -w_{,x}(x,b)\frac{x}{a} \tag{56}$$

$$M'_y(x,b) = \dot{M}_y(x,b) - M_{y,x}(x,b)\mathcal{V}_x(x,b) = -M_{y,x}(x,b)\frac{x}{a} \tag{57}$$

$$\psi'_y(x,b) = \dot{\psi}_y(x,b) - \psi_{y,x}(x,b)\mathcal{V}_x(x,b) = -\psi_{y,x}(x,b)\frac{x}{a} \tag{58}$$

Nastran SOL 400 was used to conduct the nonlinear static analysis on a 40-by-40 mesh of CQUAD4 bilinear elements. SGR was used to approximate the spatial derivatives that appear in the local CSE boundary conditions. Five-layer patches and fourth-order Taylor series expansions were used to conduct the SGR. Figure 8 illustrates a five-layer patch and a fourth-order Taylor series reconstruction of transverse displacement used to approximate the first-order spatial derivatives of transverse displacement at a particular node.

Figure 9 shows the displacement response. The dots represent the result at the finite element nodes, the surface is an interpolation of the finite element solution, and the grey, transparent surface is the linear static solution previously presented in Cross and Canfield (2013).

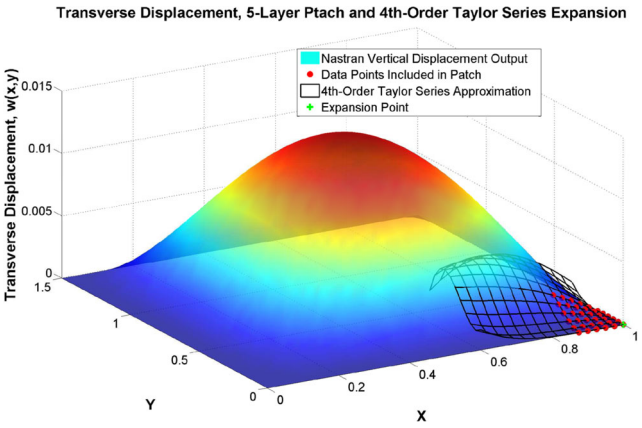

Fig. 8 SGR of vertical displacement employed with a five-layer patch and fourth-order Taylor series expansion

The coupling between the in-plane and out-of-plane degrees of freedom result in a hardening nonlinearity, making the deformations for each of the primary out-of-plane degrees of freedom roughly 55 percent smaller than the linear result (Cross and Canfield 2013). For nonlinear static analysis, Nastran does support element force output. Therefore, all of the output required to conduct local CSA with SGR can be obtained from the Nastran analysis. Figures 10 and 11 show the local and total design derivative solutions with respect to the plate dimension in the x-direction, a. The color surfaces represent the local CSA solutions with SGR, and the blue dots represent the finite difference solutions using a 10^{-4} relative step size. A relative step size of 10^{-4} was determined to be optimal for linear static plate bending using Nastran analyses by a convergence study of finite difference calculations. Smaller step sizes in Nastran introduced numerical round-off error or went unrecognized due to single precision calculations. This step size was determined to be converged for nonlinear problems as well.

The nonlinear plate response is less sensitive to the design parameter than the linear response. This is the expected result, given that the nonlinear response of the plate is stiffer than the linear response of the plate. The total design derivatives of the nonlinear response are roughly 80 percent smaller than the total design derivatives of the linear response (Cross and Canfield 2013). Quantifying the accuracy is difficult, because an analytic solution is not available for the nonlinear response. However, the absolute percent relative differences between local CSA and finite difference design derivatives were calculated using (24). The results of this calculation, shown in Table 2, demonstrate a strong agreement between the different calculations.

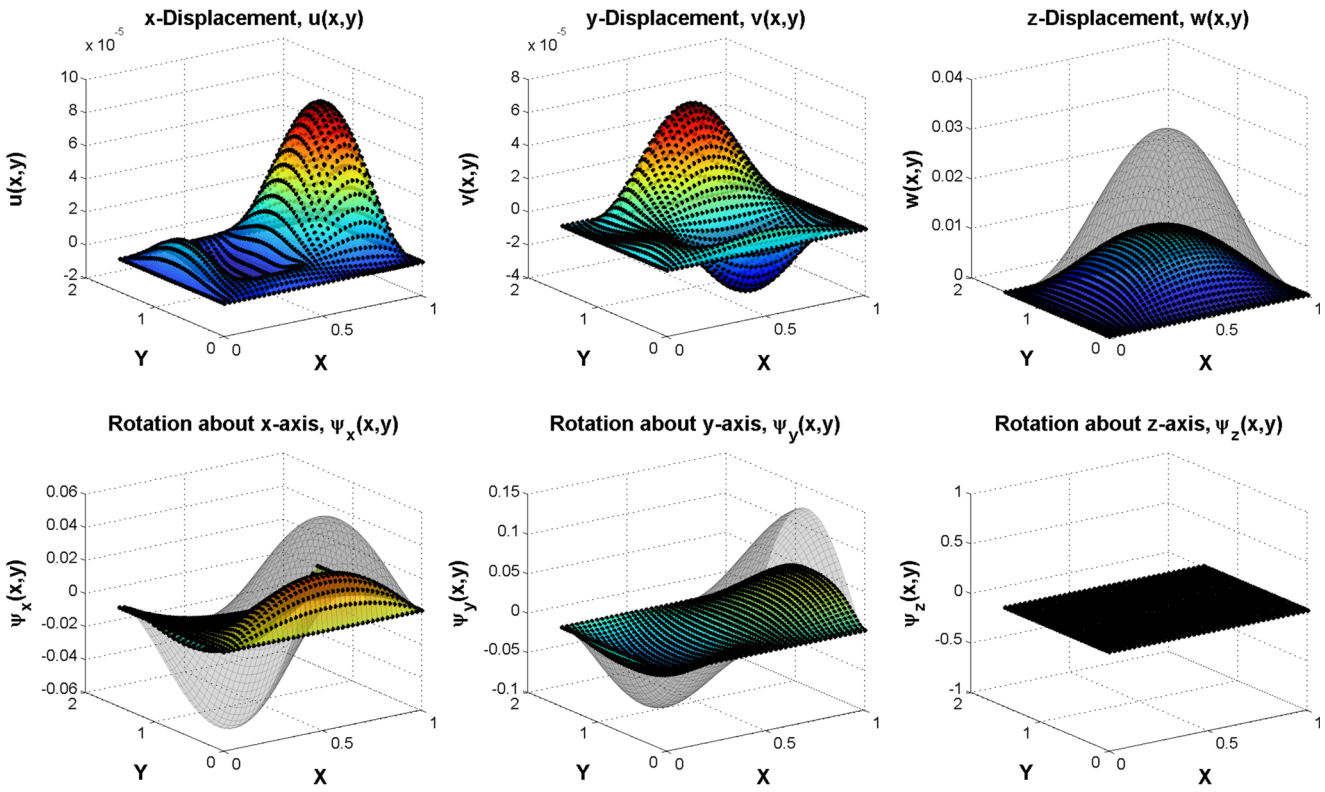

Fig. 9 Displacements of a rectangular plate with two adjacent edges clamped and the other two adjacent edges simply-supported (*grey surface*: linear analytic, *color surface*: finite element interpolation, *dots*: finite element)

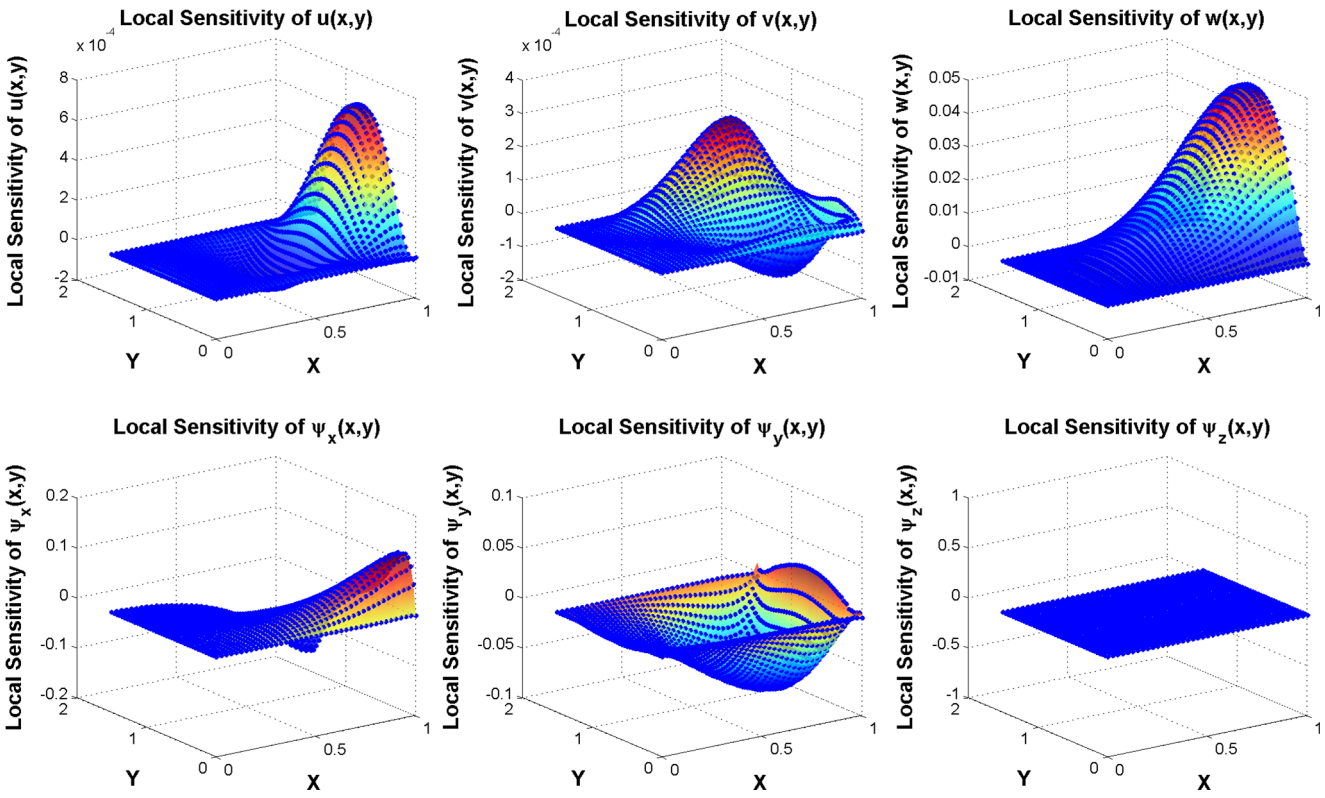

Fig. 10 Local design derivatives of displacements with respect to plate length, *a* (*color surface*: local CSA with SGR, *blue dots*: finite difference)

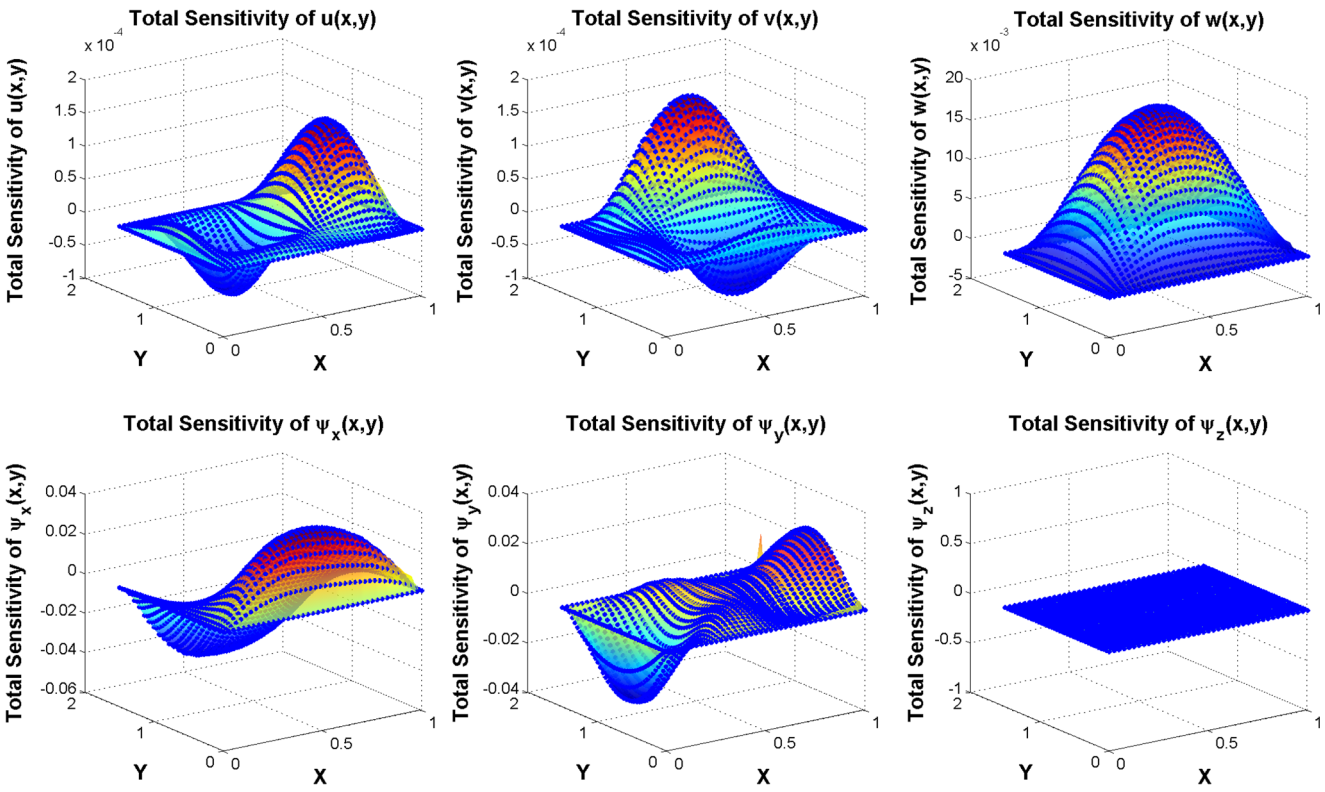

Fig. 11 Total design derivatives of displacements with respect to plate length, a (*color surface*: local CSA with SGR, *blue dots*: finite difference)

It also suggests that local CSA with SGR can be used to non-intrusively calculate design derivatives of nonlinear plate displacements.

5.2 Combined loading of a beam-stiffened plate

The same rectangular plate is now modeled with the following changes. First, all edges of the plate are simply-supported. Second, in addition to the uniformly distributed transverse load, $q_0 = 5 \times 10^4 N/m^2$, an uniformly distributed in-plane load is applied in the positive y-direction, $p_0 = 2 \times 10^6 N/m^2$. Third, the plate is modified by a stiffener that is placed along the $x = a/2 = 0.5m$ axis. The stiffener is modeled as a beam having $E = 7e10N/m^2$, $G = 26e9N/m^2$, $A = 0.0025m^2$, and $I = 1e-6m^4$. The structural nodes of the beam are coincident with the structural nodes of the plate that lie on the $x = 0.5m$ axis. The neutral axis of the beam is not offset from the nodes, but an offset would not affect the sensitivity formulation. This plate model was previously presented by Cross and Canfield (2013) for linear analysis with only out-of-plane loading. The combined loading for the nonlinear analysis creates significant coupling between the in-plane and out-of-plane degrees of freedom. For the out-of-plane degrees of freedom, the nonlinear response is roughly 15 percent stiffer (smaller) than the linear response. For the in-plane degrees of freedom, the nonlinear response is roughly 15 percent softer (larger) than the linear response. The displacement results shown in Fig. 12 illustrate the coupling effect. Nastran was used to conduct the analysis on a 60-by-40 mesh of CQUAD4 elements.

Local CSA with SGR was implemented to calculate the design derivatives of the plate displacements with respect to the plate dimension, a. The local CSE boundary conditions were derived in a similar fashion to those presented in (39) through (58). The design velocity that was used is

$$\boldsymbol{\mathcal{V}}(x, y; a) = \boldsymbol{\mathcal{V}}_x \hat{x} + \boldsymbol{\mathcal{V}}_y \hat{y} = (x/a - 1/2)\,\hat{x} \tag{59}$$

The strain discontinuities that occur at the stiffener are automatically accounted for in the local CSE system, because

Table 2 Maximum absolute percent relative difference of design derivative results

	u'	$\dot{u}$	v'	$\dot{v}$	w'	$\dot{w}$	ψ_x'	$\dot{\psi}_x$	ψ_y'	$\dot{\psi}_y$
ϵ	0.059	2.639	1.629	0.200	0.347	0.462	0.010	0.449	0.222	0.846

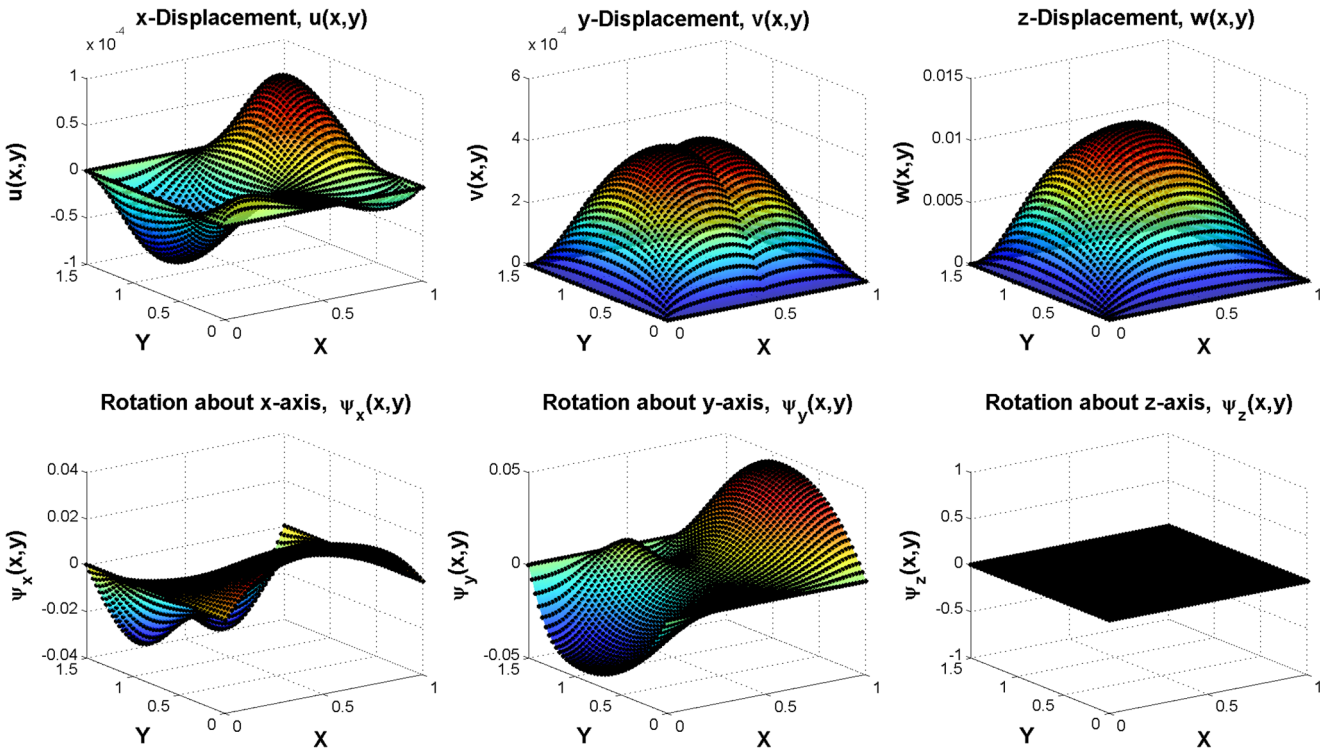

Fig. 12 Displacements of a rectangular plate with two adjacent edges clamped and the other two adjacent edges simply-supported; combined out-of-plane and in-plane loading (*surface*: finite element interpolation, *dots*: finite element)

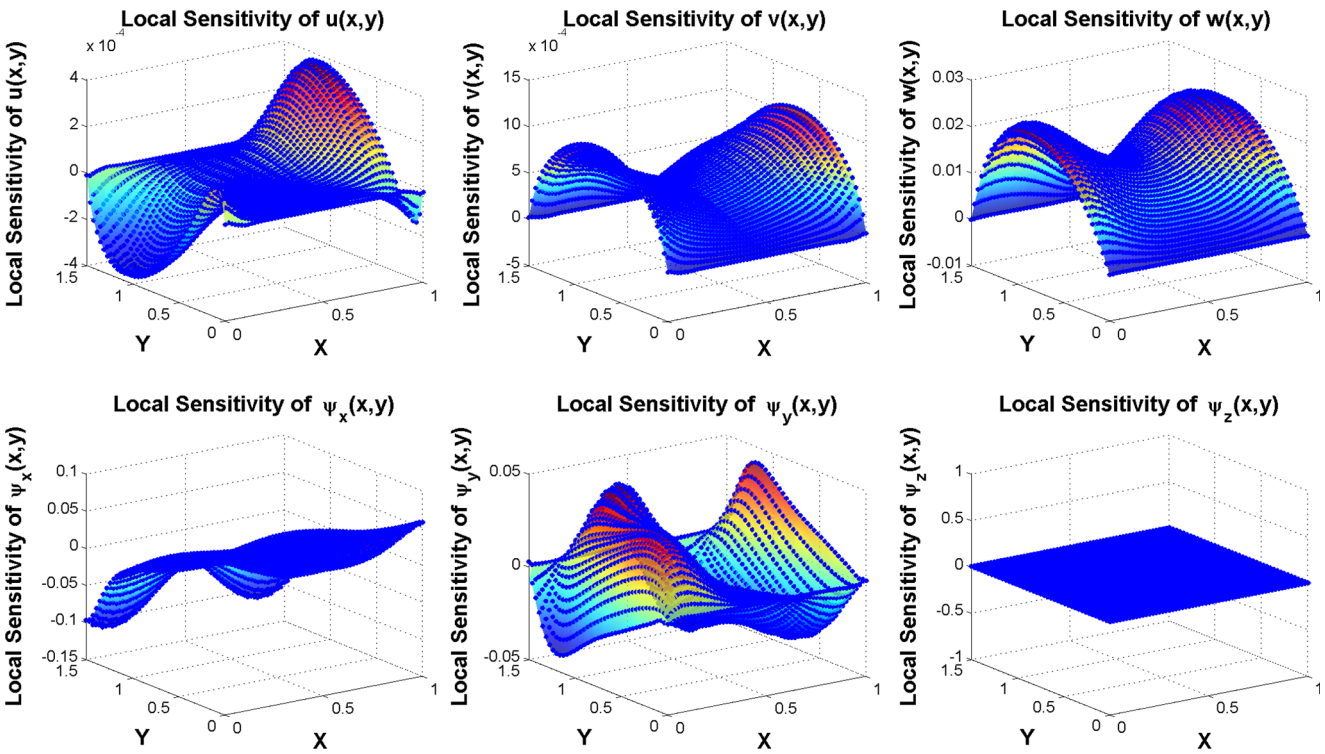

Fig. 13 Local design derivatives of displacements for plate with combined loading (*color surface*: local CSA with SGR, *blue dots*: finite difference)

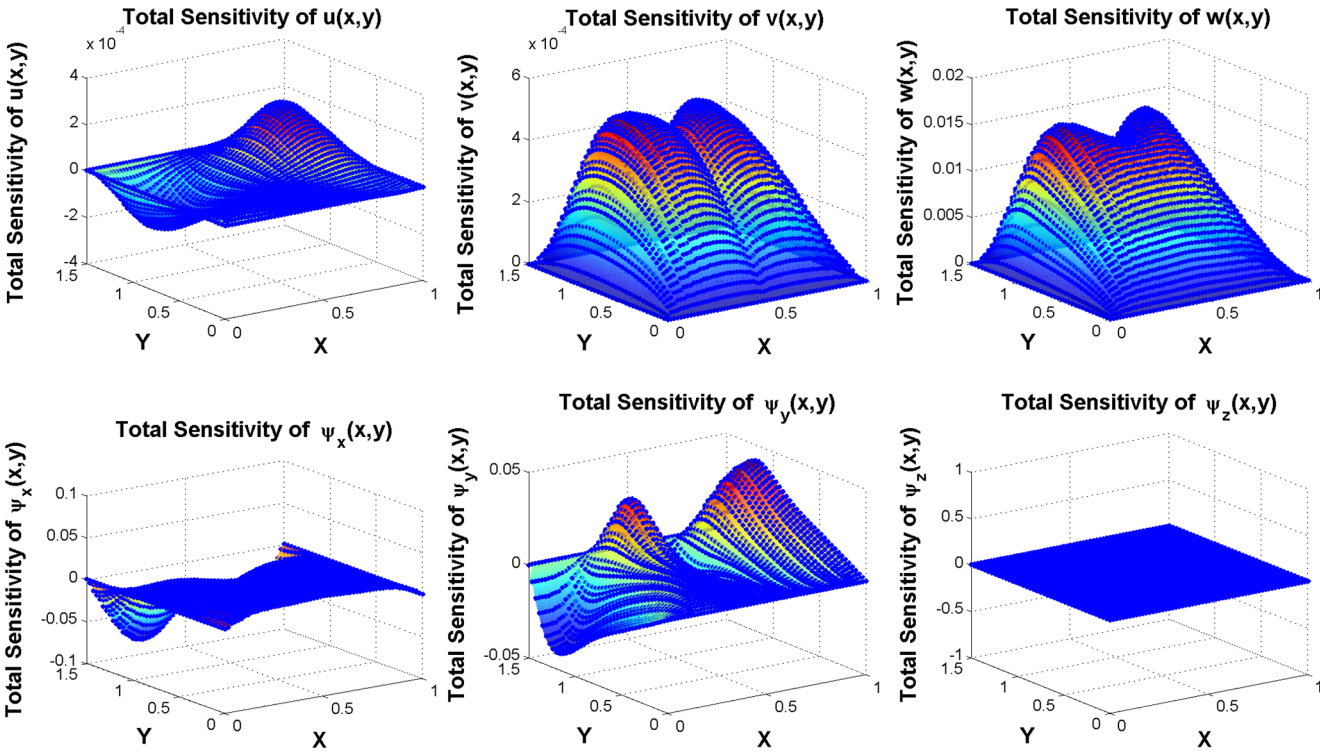

Fig. 14 Total design derivatives of displacements for plate with combined loading (*color surface*: local CSA with SGR, *blue dots*: finite difference)

Table 3 Maximum absolute percent relative difference of design derivative results

	u'	$\dot{u}$	v'	$\dot{v}$	w'	$\dot{w}$	ψ_x'	$\dot{\psi}_x$	ψ_y'	$\dot{\psi}_y$
ϵ	3.9	7.0	1.7	3.6	1.5	2.6	2.7	3.7	8.0	8.2

the design velocity at this point is equal to zero. Otherwise, non-homogeneous interface boundary conditions would be applied (Cross and Canfield 2013). Five-layer patches and fourth-order Taylor series expansions were used to conduct SGR. Figures 13 and 14 show a comparison of the local and total design derivative solutions using local CSA with SGR and finite differences with a 10^{-4} relative step size. The finite difference calculations are converged for a relative step size equal to 10^{-4}.

Due to the coupling effects and the presence of the in-plane load, the response is most sensitive to the design variable in the $0.5 < y < b$ part of the domain. Table 3 contains the maximum absolute percent relative difference between local CSA with SGR and finite difference design derivative calculations. Figures 13 and 14 and the comparison below demonstrate that local CSA with SGR can be used to nonintrusively calculate design derivatives of a nonlinear plate response using a black box tool.

6 Conclusions

The nonintrusive local continuum formulation presented in Cross and Canfield (2013) was extended to nonlinear problems. The structures community most commonly uses total CSA; one reason being that approximations of high-order derivatives of primary variables in the local CSA boundary conditions introduce error. Duvigneau and Pelletier (2006) used local CSA to calculate fluid flow design derivatives, and achieved accurate derivative approximations by using least-squares matching of Taylor series expansions to the response data. This approach has been adapted to calculate first-order derivatives of primary and secondary response variables, needed for local CSA of structural problems. This particular formulation in conjunction with SGR allows shape design derivatives to be calculated accurately, efficiently, and nonintrusively. The method was employed for nonlinear static bending of beam models that used

Euler-Bernoulli and Timoshenko beam theories. The exact same algorithm was used for each beam model and did not require any changes or modifications to the algorithm. This example demonstrates that the approach is element agnostic. The method was also used to calculate shape design derivatives of a nonlinear transient gust response of a 2-D beam model. Local CSA has not been commonly used for structural applications because of the strain discontinuities that can occur at structural interfaces. The local CSE interface boundary conditions, which account for the discontinuities, presented in Liu and Canfield (2013a), require additional spatial derivatives of the primary and secondary response variables. This example demonstrates that as long as accurate approximations of these derivatives can be obtained from the analysis output, then accurate design derivatives can be calculated using the local CSA method. Lastly, local CSA with SGR was used to calculate shape design derivatives for nonlinear static bending of a rectangular plate with mixed boundary conditions and for a beam-stiffened rectangular plate with combined loading. This example demonstrates that local CSA with SGR can be used to nonintrusively calculate design derivatives for nonlinear plate analysis in a black box tool. Furthermore, both the gust and plate examples demonstrated that nonlinear effects can have a significant effect on the design derivative solutions.

Conventional analytic sensitivity methods cannot treat the analysis tools as a black box, as numerical methods such as finite difference do, and for that reason cannot be implemented easily for nonlinear analysis conducted by a tool like Nastran. Now, the nonintrusive local CSA method with SGR can be used to more accurately calculate shape design derivatives of black box solvers. The method is limited by requiring that the analysis tool be able to provide system matrices, primary variable response data, and secondary variable response data. As evidenced by Nastran's inability to provide element force data for nonlinear transient analysis, said requirements are not always satisfied. Lastly, it was shown by Cross and Canfield (2013) that mesh refinement may be required to achieve derivative approximations that satisfy the desired error tolerance. However, Duvigneau and Pelletier (2006) show that if the analysis converges asymptotically with mesh refinement, then so will the derivative approximations by way of SGR. The authors plan to conduct further studies to quantify the effects that patch parameters have on the accuracy of local CSA with SGR.

Future work will also investigate applying the nonintrusive local CSA method with SGR to computational fluid dynamics in an effort to support shape design of systems with fluid-structure interaction (FSI). The FSI problem investigated in this research used quasi-steady typical section aerodynamics. Therefore, the design derivative of the aerodynamic load was trivial. This will not be the case when higher-fidelity aerodynamic analysis is used. All aeroelastic analyses with fluid-structure interaction possess interface conditions which govern the physical interaction between the fluid and structure. The sensitivity analysis will always require that these interface conditons be differentiated with respect to the design variables and serve as sensitivity boundary conditions. In addition, of particular interest are practical design problems with many design variables, where adjoint methods are much more efficient than direct methods. For static and steady state problems, Kulkarni et al. (2014) have extended the nonintrusive formulation presented here to an adjoint method which is well suited for large-scale design problems. The development of nonintrusive CSA using an adjoint for transient problems is a subject of ongoing research.

Acknowledgments This material is based on research sponsored by Air Force Research Laboratory under agreement number FA8650-09-2-3938. The U.S. Government is authorized to reproduce and distribute reprints for Governmental purposes notwithstanding any copyright notation thereon. The authors gratefully acknowledge the support of AFRL Senior Aerospace Engineers Dr. Raymond Kolonay, Dr. Ned Lindsley, and Dr. Jose Camberos.

References

Arora J, Haug E (1978) Design sensitivity analysis of elastic mechanical systems. Comput Methods Appl Mech Eng 15:35–62

Arora J, Haug E (1979) Methods of design sensitivity analysis in structural optimization. AIAA J 17(9):79–4109

Borggaard J, Burns J (1994) A sensitivity equation approach to shape optimization in fluid flows. Technical Report, Langley Research Center

Borggaard J, Burns J (1997) A pde sensitivity equation method for optimal aerodynamic design. J Comput Phys:136

Choi K, Kim NH (2005) Structural sensitivity analysis and optimization. Springer Science + Business Media

Cross D, Canfield RA (2012a) Solving continuum shape sensitivity with existing tools for nonlinear aeroelastic gust analysis. In: 53rd AIAA/ASME/ASCE/AHS/ASC structures, structural dynamics, and materials conference. AIAA, Honolulu, pp 2012–1923

Cross D, Canfield RA (2012b) Continuum shape sensitivity with spatial gradient reconstruction of nonlinear aeroelastic gust response. In: 14th AIAA/ISSMO multidisciplinary analysis and optimization conference. AIAA, Indianapolis, pp 2012–5597

Cross D, Canfield RA (2013) Local continuum shape sensitivity with spatial gradient reconstruction. Struct Multidiscip Optim J. (accepted with revisions)

Dems K, Haftka R (1989) Two approaches to sensitivity analysis for shape variation of structures. Mech Struct Mach 4:16

Dems K, Mroz Z (1985) Variational approach to first- and second-order sensitivity analysis of elastic structures. Int J Numer Methods Eng 21

Duvigneau R, Pelletier D (2006) On accurate boundary conditions for a shape sensitivity equation method. Int J Numer Methods Fluids 50

Etienne S, Pelletier D (2005) General approach to sensitivity analysis of fluid-structure interactions. J Fluids Struct 21:2

Haftka RT, Adelman HM (1989) Recent developments in structural sensitivity analysis. Struct Optim I

Haug EJ, Arora JS (1978) Design sensitivity analysis of elastic mechanical systems. Comput Methods Appl Mech Eng 15:35–62

Jameson A (1988) Aerodynamic design via control theory. J Sci Comput 3:233–260

Johnson FP (2001) Sensorcraft–tomorrow's eyes and ears of the warfighter. AIAA modeling and simulation technologies conference and exhibit. AIAA-2001-4370

Kulkarni MD, Cross DM, Canfield RA (2014) Discrete adjoint formulation for continuum sensitivity analysis. Technical note submitted to AIAA Journal

Liu S, Canfield RA (2012) Continuum shape sensitivity method for fluid flow around an airfoil. In: 53rd AIAA/ASME/ASCE/AHS/ASC structures, structural dynamics, and materials conference. AIAA, Honolulu, pp 2012–1426

Liu S, Canfield RA (2013a) Boundary velocity method for continuum shape sensitivity of nonlinear fluid-structure interaction problems. J Fluids Struct

Liu S, Canfield RA (2013b) Two forms of continuum shape sensitivity method for fluid-structure interaction problems. To appear in AIAA J

Liu S, Canfield RA (2013c) Equivalence of continuum and discrete analytic sensitivity methods for nonlinear differential equations. To appear in Struct Multidiscip Optim J

Liu S, Wickert PD, Canfield RA (2010) Fluid-structure transient gust response sensitivity for a nonlinear joined wing model. In: 51st AIAA/ASME/ASCE/AHS/ASC structures, structural dynamics, and materials conference. AIAA, Orlando, pp 2010–3118

MSC Software Corporation. Md nastran 2010: User defined services. MD Nastran Documentation (2010)

NASA Helios prototype. nasa dryden flight research center (2004). http://www.nasa.gov/centers/dryden/news/ResearchUpdate/Helios/index.htm l. Online; Accessed 27 Aug 2013

Stanley L, Stewart D (2002) Design sensitivity analysis: computational issues of sensitivity equation methods. Academic Press

Turgeon E, Pelletier D, Borggaard J (1999) A continuous sensitivity equation approach to optimal design in mixed convection. AIAA:99–3625

Wickert DP (2009) Least-squares, continuous sensitivity analysis for nonlinear fluid-structure interaction. Dissertation, Air Force Institute of Technology

Wickert DP, Canfield RA (2008) Least-squares continuous sensitivity analysis of an example fluid-structure interaction problem. In: 49th AIAA/ASME/ASCE/AHS/ASC structures, structural dynamics, and materials conference. AIAA, Schaumberg, pp 2008–1896

Wickert DP, Canfield RA, Reddy JN (2008) Continuous sensitivity analysis of fluid-structure interaction problems using least-squares finite elements. In: 12th AIAA/ISSMO multidisciplinary analysis and optimization conference. AIAA, Victoria, pp 2008–5931

Wickert DP, Canfield RA, Reddy JN (2009) Fluid-structure transient gust sensitivity using least-squares continuous sensitivity analysis. In: 50th AIAA/ASME/ASCE/AHS/ASC structures, structural dynamics, and materials conference. AIAA, Palm Springs, pp 2009–2535

Zienkiewicz OC, Zhu JZ (1992) The superconvergent patch recovery and a posteriori error estimates. part 1: the recovery technique. Int J Numer Methods Eng 33